Available online at www.sciencedirect.com
ScienceDirect
Earth and Planetary Science Letters 265 (2008) 423–437
EPSL
www.elsevier.com/locate/epsl

On the statistical distribution of seismic velocities in Earth's deep mantle

John W. Hernlund [a,*], Christine Houser [b]

[a] Institut de Physique du Globe de Paris, 4 Place Jussieu, 75252 Paris, Cedex 05, France
[b] Earth and Planetary Sciences, University of California Santa Cruz, 1156 High Street, Santa Cruz, CA, 95064 USA

Received 11 August 2007; received in revised form 18 October 2007; accepted 18 October 2007
Available online 1 November 2007
Editor: C.P. Jaupart

Abstract

The existence of uncoupled shear (S) and compression (P) wave velocity variations in Earth's mantle is a characteristic that might only be explained by the presence of significant chemical and/or phase heterogeneity, with important implications for the dynamics and evolution of Earth's interior. While making a one-to-one comparison between tomographic models for P and S velocity (V_P and V_S) variations for a particular geographic region is ill-posed, their global statistical distributions reveal several robust characteristics indicative of the nature of uncoupled V_P and V_S in the deep mantle. We find that all of the V_P and V_S model distributions at a given depth are Gaussian-like throughout the lowermost mantle. However, a distinct low velocity feature is present in V_S distributions below $\approx$2200 km depth that is not present or is relatively weak in V_P models. The presence of anomalously low V_S material cannot be explained as an artifact, nor can the absence of a similarly strong feature in P models be ascribed to under-resolution. We propose that this feature can be partly explained by laterally variable occurrences of post-perovskite (pPv) lenses in the D'' layer, however, the persistence of significantly slow V_S regions at heights up to $\approx$700 km or more above the core–mantle boundary is likely to be incompatible with a pPv origin and might only be explained by the presence of a laterally discontinuous layer of chemically distinct material and/or some other kind of phase heterogeneity. There also exist significant discrepancies between tomographic models with respect to the width of the distributions as well as differences between the modeled peak values. We propose a scheme for comparison between different seismic models in which the widths of the dominant features in their statistical distributions is exploited.

Keywords: core–mantle boundary; seismic tomography; D''; lower mantle; mantle convection; chemical heterogeneity; post-perovskite

1. Introduction

To a good approximation Earth's mantle is spherically-symmetric, where the largest changes in physical properties such as seismic velocity occur with increasing pressure/depth toward the center (Bullen, 1949; Birch, 1952; Dziewonski and Anderson, 1981). Models for lateral variations in the velocity of propagated shear (V_S) and compressional (V_P) waves in Earth's mantle are typically obtained by tomographic inversion of observed travel times for various seismic phases recorded at global seismic stations relative to those predicted by one-dimensional radial Earth models. The resulting V_S and

* Corresponding author. Currently at: Department of Earth and Ocean Sciences, University of British Columbia, 6339 Stores Road, Vancouver, Canada V6T 1Z4.
E-mail address: hernlund@gmail.com (J.W. Hernlund).

0012-821X/$ - see front matter © 2007 Elsevier B.V. All rights reserved.
doi:10.1016/j.epsl.2007.10.042

V_P tomography models contain important information regarding three-dimensional temperature, phase, and composition variations in the Earth's mantle. Of particular interest are differences in variations of V_S relative to V_P, which are a primary indication of Earth structure that might not be explicable by temperature variations arising from mantle convection alone. Such regions of anomalous V_S and V_P variations are vital to interpreting the dynamical evolution, composition, and current state of Earth's deep interior.

Many techniques have been called upon to distill relative V_S and V_P variations in the Earth's deep mantle. The most basic approach involves comparison of the total relative amplitude of lateral variations in V_S and V_P with depth in the mantle based on the estimation of a correlation parameter $R = \delta \ln V_S / \delta \ln V_P$ (Vasco et al., 1994; Robertson and Woodhouse, 1995, 1996; Su and Dziewonski, 1997; Kennett et al., 1998; Masters et al., 2000; Saltzer et al., 2001; Ritsema and van Heijst, 2002), and most studies find an increase in the value of R with increasing depth in the lowermost mantle. A significant jump in R is correlated with increased seismic heterogeneity in the D'' region, and this has been proposed to arise from the existence of dense thermo-chemical structures at the base of the mantle (Tackley, 1998; Davaille et al., 2003; McNamara and Zhong, 2004). Another approach arises from evaluating the probability of thermal vs. chemical heterogeneity from a suite of models that is consistent with available mineral physics and seismic data; this procedure consistently yields indications of large-scale chemical and/or phase heterogeneity in Earth's deep mantle (Beghein et al., 2002; Trampert et al., 2004).

Others have considered the relative geographic patterns of inferred density, bulk sound speed, and shear velocity in the lowermost mantle to identify regions where an anti-correlation of bulk sound speed and shear velocity may be associated with structures having an intrinsically higher density (Masters et al., 2000; Ishii and Tromp, 2004). A variety of individual ray paths may also be used to delineate regions of anomalous seismic velocities (e.g., Wang and Wen, 2004) where rapid lateral variations likely cannot be explained as thermal in origin (Wen, 2001; Ni et al., 2002). Another methodology assumes a relationship between seismic shear velocity and density variations in the mantle, which is supplemented by the calculated pattern and strength of flow based upon a viscous deformation model for comparison to the geoid, plate velocities, dynamic topography, or other derived information that are used as additional constraints (e.g., Hager and Clayton, 1989; Forte and Mitrovica, 2001). The latest approach (Simmons et al., 2006) jointly inverts for shear velocity and density in order to determine whether low V_S features in the deep mantle are buoyant or whether compositional contributions are required (Simmons et al., 2007). This more general problem is subject to additional complexity because it introduces sensitivity to other uncertain mantle properties such as rheology, although the results are usually consistent with those obtained by other approaches.

While increasingly complex models carry great promise for resolving some of the issues in uniquely determining the origin of mantle heterogeneity, the models for seismic velocity variations themselves are not yet thoroughly understood. It is therefore worthwhile to attempt a further distillation of these models to better quantify how V_S and V_P vary in distinct ways from one another, and to understand to what extent these signals are affected by any potential artifacts arising from tomographic inversions. Previous studies of the gross statistics of travel-time residuals for direct phases at different turning depths revealed that V_S and V_P vary in distinct ways in the lowermost mantle, with particularly strong delays in S arrivals for waves turning in the mid-Pacific deep mantle (Bolton and Masters, 2001; Saltzer et al., 2001). This kind of analysis was performed using the most raw form of available seismic data, and is able to provide robust indications of the existence of uncoupled V_S and V_P variations without reference to tomographic inversions. Yanagisawa and Hamano (1999) studied the statistical distribution of V_S anomalies from a single tomographic model at various depths in the mantle, and noted a "skewness" that appears due to the large low shear velocity provinces (LLSVP) beneath the Pacific and Africa in the deepest mantle. By comparison with mantle convection models, they argued that this V_S skewness can be explained by a stronger degree of core cooling relative to the degree of internal heating by radioactive decay in the mantle. However, the degree of internal heating in Earth's mantle is thought to be relatively large based upon estimates of the total budget of incompatible heat producing elements (Hofmann, 1997). This previous study also did not simultaneously consider V_P models, for which similar statistical features should be observed if attributed to a purely thermal origin.

Here we extend the work of Yanagisawa and Hamano (1999) to the distribution of seismic velocity anomalies from both V_S and V_P tomographic inversions of short and long-period travel-time residuals. We find that the previously reported "skewness" in V_S assumes the form of a nearly bi-modal distribution, where a low V_S tail is super-imposed upon an otherwise dominantly Gaussian variation. This is a robust and ubiquitous feature present in a variety of S tomography models at depths greater

Table 1
Summary of primary data used for *S* inversions

Model	*S*	*SS*	SSS_{etc}	*ScS*	S_{diff}	*SKS*	*SKKS*	*SS–S*	*ScS–S*	S.W.	N.M.S	Waveforms
J362D28	X							X	X	X		X
HMSL-S06	X	X						X	X	X		
S20RTS	X	X	X	X	X	X				X	X	
TX2006	X	X	X	X		X	X					
PRI-S05	X							X	X			
SAW24B16												X

S.W. is surface waves and N.M.S. is normal mode splitting.

than about 2200 km. However, this kind of feature is absent in V_P models, and we find that this cannot be simply explained by a lack of resolution. By decomposing the distributions, we estimate the volume of material responsible for producing the low V_S features, yielding a value of about 2.0±0.4% of the total mantle volume. In model distribution comparisons there exist significant discrepancies in the amplitude of velocity variations among the suite of models examined in this study. In particular, we find that relative V_S and V_P model amplitudes vary by at least a factor of 4 among the suite of possible model pairs. We propose a model comparison strategy that uses a linear transformation that aligns and scales dominant features of the distributions to one another, although actual amplitudes cannot be confidently recovered by any procedure. Baseline shifted and scaled V_S and V_P models based on a similar mapping between their statistical distributions reveals that post-perovskite lenses may exist both in high velocity regions of the mantle underlying previous subduction zones as well as inside the large low shear velocity regions, although this latter feature is not sufficiently resolved by *P* tomography models at the present time.

2. Statistical distributions of tomographic models

The models analyzed here represent the latest developments in seismic tomography of the Earth's mantle. The goal of each of these models is to maximize the resolution of mantle structures from the surface to the CMB, which is accomplished by increasing the size and variety of the *S* phase datasets or by applying more sophisticated theory than previous models. The *S* velocity models include SAW24B16 from Megnin and Romanowicz (2000), S20RTS from Ritsema and H.J. (2000), J362D28 from Antolik et al. (2003), PRI-S05 from Montelli et al. (2006), TX2006 from Simmons et al. (2006), HMSL-S06 from Houser et al. (submitted for publication), and the average model SMEAN from Becker and Boschi (2002). All the models are based on long-period *S* phases. The datasets used in each of the models are indicated in Table 1 and the individual methodologies are shown in Table 2. S20RTS uses a fully automated picking method to determine the arrival times of *S* phases. HMSL-S06 applies a semi-automated picking method to determine *S* and *SS* arrival times as well as including the *SS–S* and *ScS–S* (updated through 2004) travel times of Masters et al. (2000). TX2006 uses fully manual picks for many direct and depth *S* phases. The PRI-S05 model is based on the manual *S*, *SS–S*, and *ScS–S* picks from Masters et al. (2000) while J362D28 uses the direct and differential picks of Liu and Dziewonski (1998), the surface wave dispersion measurements of Ekstrom et al. (1997), and the waveform fitting of Gu et al. (2001). SAW24B16 uses waveforms and non-linear asymptotic coupling theory while J362D28 uses the path averaged approximation (Woodhouse and Dziewonski, 1984) for their waveform modeling. S20RTS, TX2006, and HMSL-S06 use ray theory to map the sensitivity of the *S* phases within the Earth while the PRI-S05 model uses finite frequency kernels. In order to account for upper mantle

Table 2
Summary of inversion and picking methods for *S* tomography models

Model	Ray theory	Finite frequency	Manual	Auto	Semi-auto	Reference
J362D28	X		X			Antolik et al. (2003)
HMSL-S06	X				X	Houser et al. (submitted for publication)
S20RTS	X			X		Ritsema and van Heijst, 2000
TX2006	X		X			Simmons et al. (2006)
PRI-S05		X	X			Montelli et al. (2006)
SAW24B16		X	X			Megnin and Romanowicz (2000)

structure, models J362D28 and HMSL-S06 use surface waves while the TX2006 and S20RTS models use the multiples of *S* (i.e. *SS* and *SSS*) phases to constrain the upper mantle. However, TX2006 uses a larger set of multiple phases such that they are essentially measuring Love waves. The models that include waveforms also account for the upper mantle. The PRI-S05 model only uses body waves and therefore the lower mantle structure of their model may be influenced by artifacts of the upper mantle. The mantle models are parameterized by rectangular blocks (S20RTS, TX2006, and HMSL-S06), splines (J362D28 and SAW24B16), or an irregular Delaunay mesh (PRI-S05). In addition, each of the models is very dependent on the regularization (i.e., smoothing) of the initially stiff (i.e., nearly singular) inverse problem. SMEAN is not an actual tomographic model, but rather a harmonically averaged suite of older V_S models analyzed by Becker and Boschi (2002).

Several of the *S* models have corresponding *P* models; J362D28 from Antolik et al. (2003), PRI-P05 from Montelli et al. (2004), HMSL-P06 from Houser et al. (submitted for publication), and PMEAN from Becker and Boschi (2002). The parameterizations and inversion methods for the *P* models are the same as their respective *S* models. We also include a short-period *P* model (MIT-P07) from Li and van der Hilst (in press) which is based on the millions of *P* travel times recorded by the International Seismic Centre (ISC). This latest MIT model uses ray theory, but has a much finer block-style parameterization than the other *P* models. The datasets used in each of the models are indicated in Table 3. HMSL-P06 uses a semi-automated picking method to determine *P* and *PP* travel times, but also the manual *PP–P* picks of Masters et al. (2000). The PRI-P05 model is based on the *P* and *PP–P* times from Masters et al. (2000), but uses finite frequency kernels. J362D28 is a joint *S* and *P* model that uses summary rays based on the short-period ISC *P* picks, waveforms from Gu et al. (2001), and the *PP–P* times from Masters et al. (2000). PMEAN is not actually a model, but a composite of the older *P* models analyzed by Becker and Boschi (2002) and obtained by averaging, after spherical-harmonic filtering, of a suite of models. All the long-period *P* models share the problem that there is essentially zero sensitivity of surface waves to compressional velocity, so there exists little constraint on upper mantle structure and artifacts from the upper mantle may be mapped into the lower mantle.

Table 3
Summary of primary data used for *P* inversions

Model	*P*	*PP*	*pP*	*PP–P*	Waveforms
J362D28	X			X	X
HMSL-P06	X	X		X	
PRI-P05	X			X	
MIT-P07	X		X	X	

Distributions of seismic velocity were obtained by calculating the % area at natural discretization depths for each tomography model by summing over the cosines of the latitude of the model value after transferring the models to a uniform spherical polar grid. The complete suite of results for both V_P and V_S models can be found in Fig. 1. The statistical distributions reveal indications of a substantial slowing in V_S relative to V_P as a distinct feature of the tomographic models. In particular, distributions of V_S and V_P anomalies are well-described by a single Gaussian at all depths, with the exception that a low velocity tail appears in V_S below about 2200 km depth, increasing in both velocity amplitude and areal abundance toward the CMB where the distribution is essentially bi-modal. All recent V_S models we have examined share this same feature, which is not best-described as a "skewness" because it manifests itself as a distinct feature apart from the primary modal variation rather than an enhanced asymmetry of a single mode. We also note that even though the velocity amplitudes, or widths of the distributions, vary significantly between the various models they are essentially self-similar in the sense that they can be aligned and scaled to fit one another. This is a characteristic that we later exploit in our discussion of model comparisons.

The Gaussian shape of the primary peak in these models provides for a unique characterization that other global measures such as the higher moments of the distributions cannot capture given the bi-modal nature of V_S at greater depths, and we are therefore motivated to better quantify this feature. For comparison, Fig. 1 also shows standard Gaussian functions (with mean μ and standard deviation σ) obtained by least squares fitting to those portions of the distributions that are "Gaussian-like." While any attempt to delineate such Gaussian-like portions of the distributions is admittedly subjective, the quality of this description is compelling. Given the overlap between the Gaussian features and the low V_S tails, we have attempted to isolate the Gaussian feature by fitting only those portions of the distributions to a standard Gaussian function for velocities greater than $\mu - 3\sigma/2$ (this is necessarily iterative, since σ and μ are not initially known) because the higher velocity portions of the distributions are "Gaussian-like" and the low velocity tails lie below values typically less than about $\mu - 3\sigma/2$. Information derived from these Gaussian fits is shown for each histogram in Fig. 1.

The distinct low V_S tail below about 2200 km depth is a robust feature that cannot be explained by artifacts in

the tomography models. In fact, the primary effect of factors such as model damping and misaligned reference velocity is to diminish, rather than enhance, this feature. However, it is important to consider if the feature actually exists in V_P within the real Earth, but is not present in the models due to differences in coverage. This would be the case, for example, if the V_P variations were not well-resolved in the regions showing the lowest V_S anomalies. To test whether geographical regions of low V_S are adequately covered by P seismic wave paths to reveal a similarly low V_P tail, we have performed a resolution test for V_P using the V_S model as input. While *ScS* provides better resolution for *S* models in the CMB region, we also find that the coverage of direct P waves is sufficient to reveal large-scale low V_P anomalies because a similarly strong low velocity

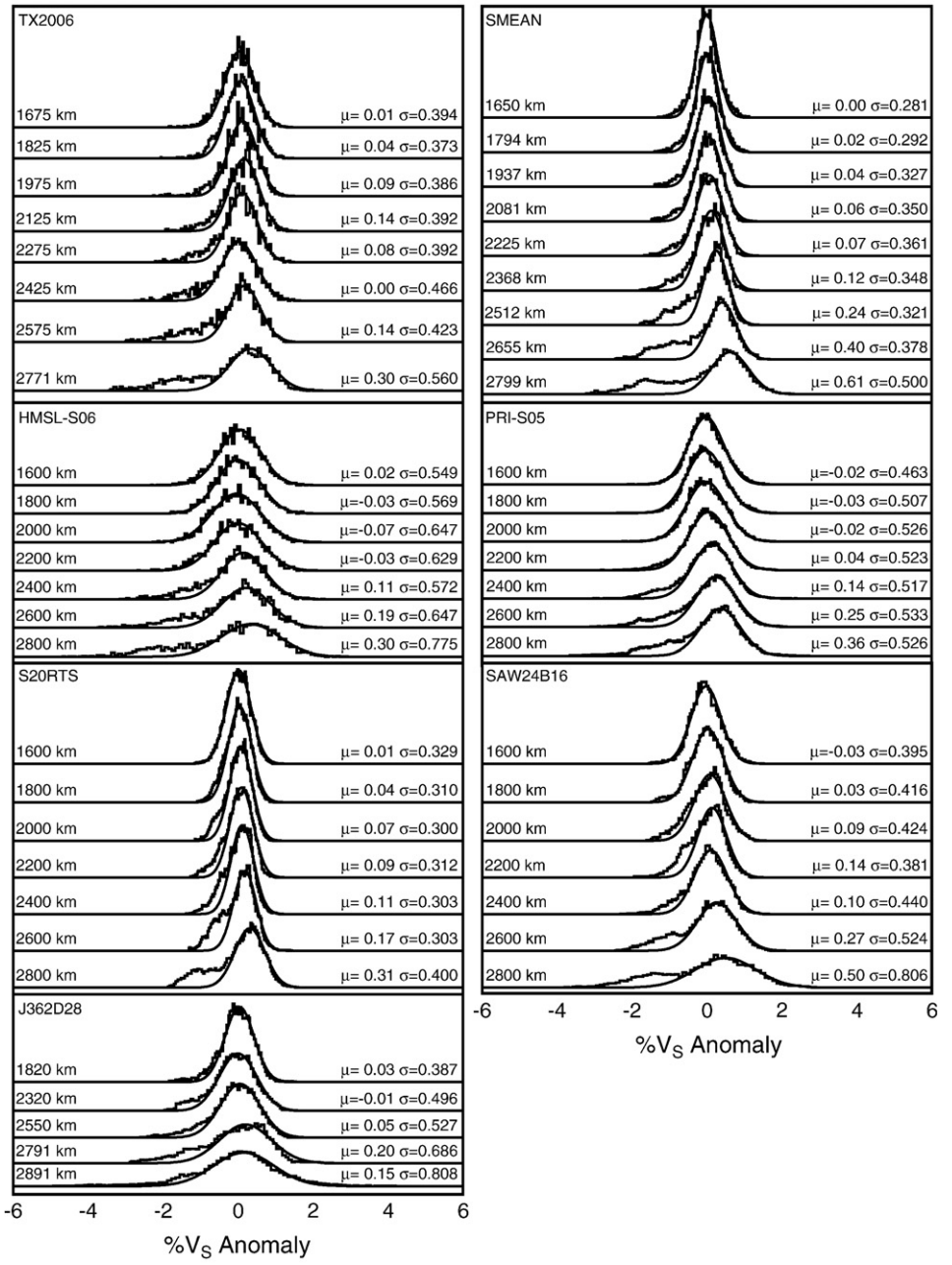

Fig. 1. Distribution of seismic velocities from the mid-mantle to the core–mantle boundary. Gaussian fits to the main peaks of the distributions are also plotted (see the text for details), along with best-fitting parameters μ and σ at each depth (see Table 2 for the list of models and references).

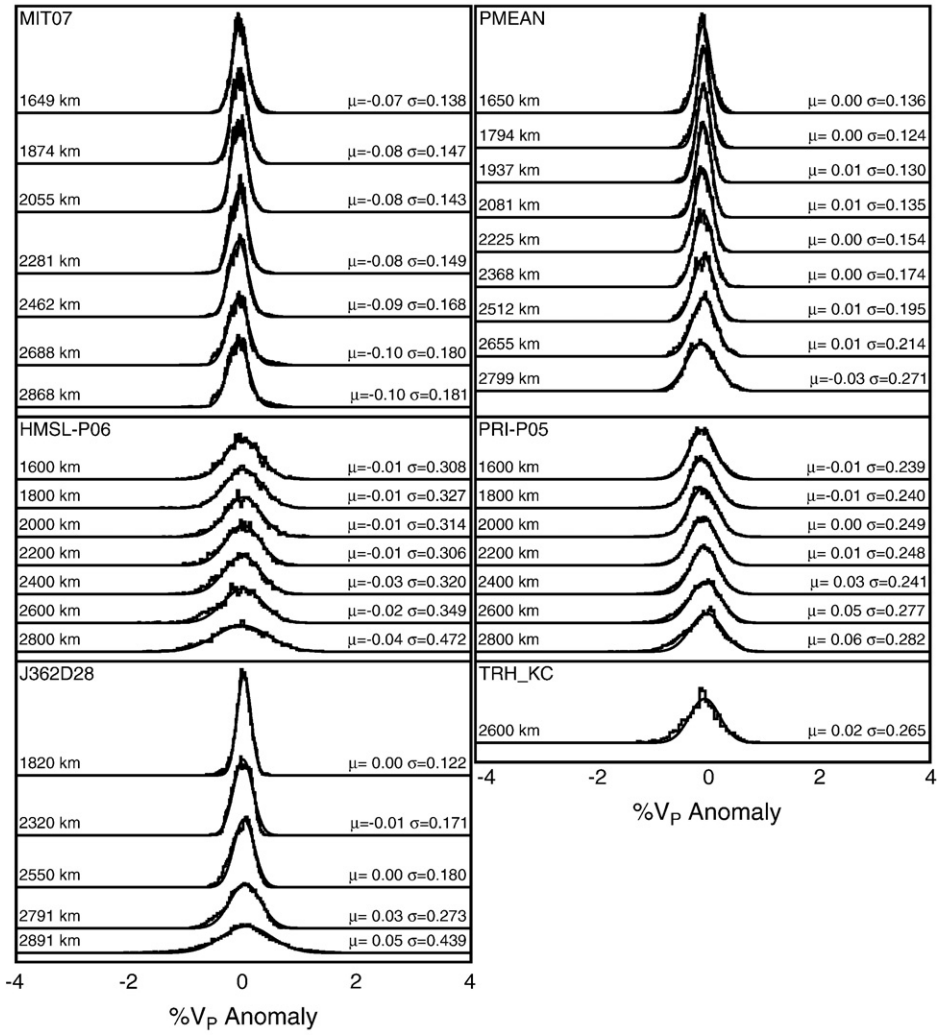

Fig. 1 (*continued*).

feature is always present in synthetic distributions of V_P obtained by this procedure. Therefore the absence of a similarly strong low V_P tail in the distributions is a robust indication of decoupling in V_S and V_P variations at the lowest seismic velocities.

3. Discussion

In the following we explore the implications of the seismic velocity distributions from the suite of tomographic models. We begin with an analysis of the variations in quantitative measures for the dominant features of the distributions and their implications for comparison of model amplitudes and baseline values. A simple linear transformation is proposed that scales each model in such a way that its distribution conforms with other models, and this scheme is also applied to the comparison of shear and compressional wave speed variations. We then turn to potential mechanisms for explaining the observed features of the distributions, including the Gaussian-like nature of much of the models and a variety of causative mechanisms for the low V_S tail.

3.1. Comparative analysis of the distributions

The most basic feature of the distributions is that much of the data are well-described as Gaussian in form, including the deep V_S velocity variations apart from the low velocity tails. Because this basic feature is also seen in the distribution of travel-time anomalies turning at

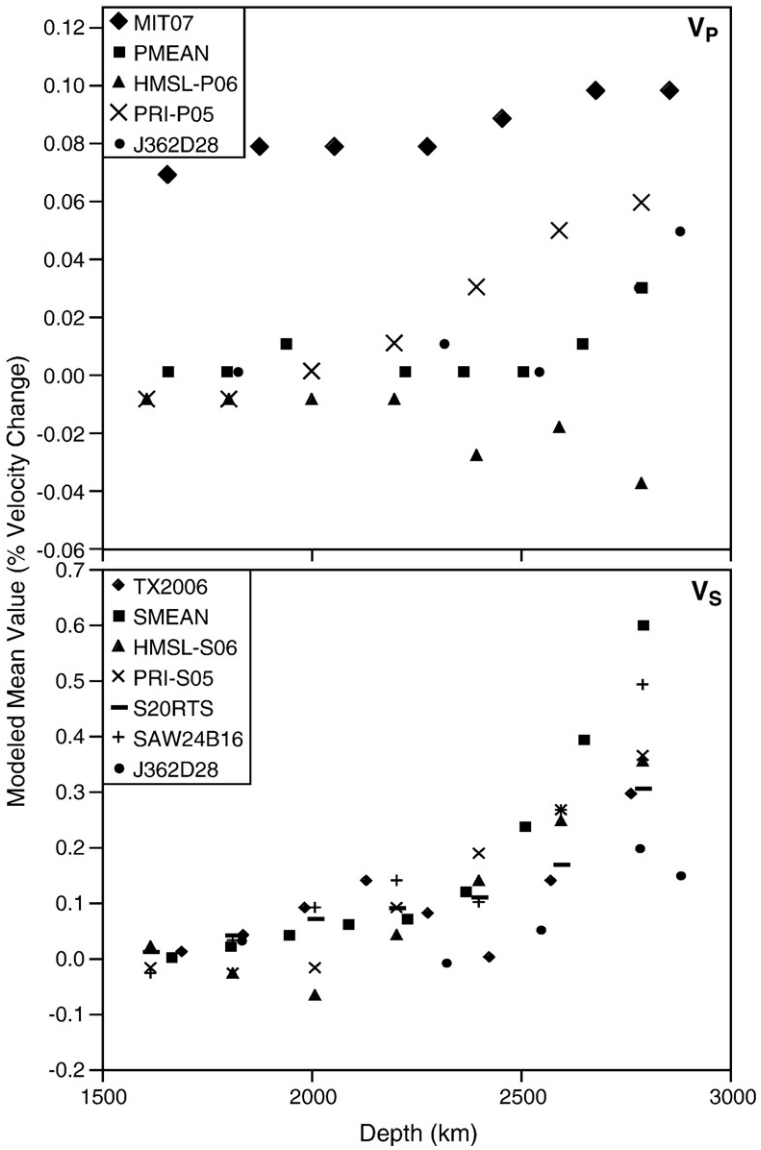

Fig. 2. Plots of the modeled peak amplitude of the Gaussian fit for each distribution as a function of depth for every tomographic model analyzed in this study (see Table 2 for the list of models and references).

this range of depths (Bolton and Masters, 2001), we posit that raw travel-time statistics map linearly into the tomographic inversions derived from these datasets and the model-dependent inversion kernels. This would then revert to a question regarding why travel-time delay statistics are mostly Gaussian to begin. This is a less straightforward question to address, since biases are sure to enter the data given the heterogeneous sampling of Earth by seismic waves. For example, by ray-tracing through mantle circulation models it has been shown that for many event-station pairs the seismic wave paths sample more cold/fast material than is typically present in the models (Davies and Bunge, 2001). This would predict that the statistics could be skewed toward faster velocities, however, the above distributions reveal surprisingly symmetric features apart from the low V_S tails below 2200 km depth.

The Gaussian fit provides a robust estimate of the peak position of the distributions using the value of μ because it is based upon fitting a smooth function to a large portion of data. This is therefore a characterization which avoids the problem of bin size-dependence and noise in the vicinity of the peak value in the distributions themselves. Furthermore, because all models share the dominant

Gaussian-like feature (and also because the low V_S tail differs in subtle details among different models), the value of σ obtained in the Gaussian fitting procedure should in principle be a robust measure of velocity amplitude variations between different models since it is based upon smooth fitting to the largest feature in the data.

Fig. 2 shows the modeled peak values of the Gaussian portions of the distributions, μ. The peaks of the velocity distributions, indicating the most abundant (and therefore representative) velocities at a given depth, are not typically found at a value of $\delta \ln V = 0\%$, or the "baseline value." This is not surprising given that the distributions are never exactly symmetric and the usual mean value (calculated as harmonic degree $l=0$) at a given depth would not necessarily be expected to correspond to the peak value of the distributions. A shift in peak values above the nominal baseline is pronounced for V_S models, which generally exhibit an increased positive departure with increasing depth which is only partly coincident with the onset of the low V_S tail. The largest departures in μ for V_S occur in the D'' layer, where there exist large discrepancies amongst the available one-dimensional seismic reference models typically used for tomographic inversions.

It is worth noting that the peak positions of the distributions vary among the suite of models. These values are taken directly from the models themselves, and therefore no correction has been applied for the use of different one-dimensional reference models. However, we find that differences in reference models cannot account for the observed variations, and in almost all cases worsen the disagreement in the inferred peak position of the distributions among the suite of models.

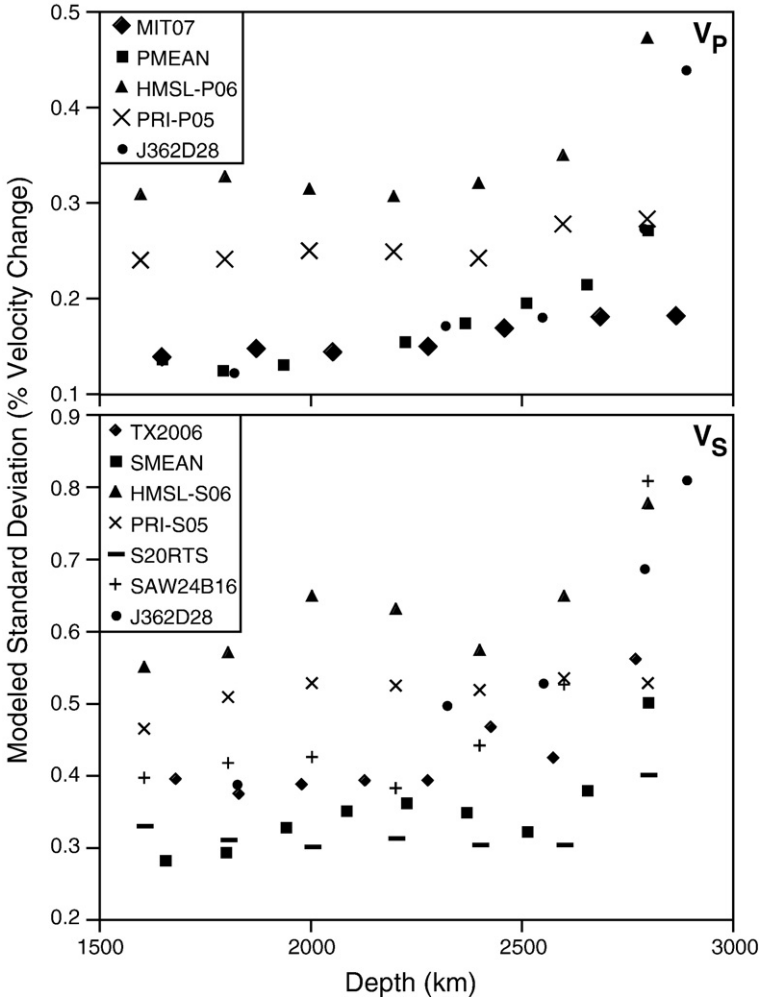

Fig. 3. Plots of the modeled standard deviation of the Gaussian fit to the main peak of each distribution as a function of depth for every tomographic model analyzed in this study (see Table 2 for the list of models and references).

For example, both MIT07 and HMSL-P06 use ak135 (Kennett et al., 1995) as a reference model, however, their peak positions fall in the uppermost and lowermost range and a simple correction accounting for the different reference model would retain this large difference as well as increase the total variations in the entire suite of models. Also, the PRI-P05 model is referenced to iasp91 (Kennett and Engdahl, 1991), which is slower in the deepest mantle than the PREM model (Dziewonski and Anderson, 1981) used by J362D28, and hence a reference model correction would further increase the differences between their peak positions. In any case, differences in V_P between the employed reference models range from about 0.2% to 0.4% at the base of the mantle, which is much larger than the observed spread in differences between the peak positions given by the models alone; indeed, these variations are larger than could be represented within the amplitude range plotted in Fig. 2. Variations in μ among the V_S models at a given depth are much larger than in the V_P models, however, they are comparable to the variations of about 0.2–0.5% between the different reference models in the deep mantle (HMSL-S06 and PRI-S05 use ak135 and iasp91, respectively, while all others use PREM). Nevertheless, like V_P, accounting for differences in the reference models does not reduce observed variations in V_S peak positions. While some pairs might be brought into better agreement by such a correction, the overall differences are not reduced.

Disagreements between the peak positions of the distributions can arise from a number of sources, and illustrates that the baseline values of tomographic models are not necessarily well-defined with respect to the employed one-dimensional reference model. One issue is that in some models (e.g., HMSL) the travel-time residuals themselves have been de-meaned prior to inversion, which ensures a decoupling between inverted values and the reference model that would be difficult to re-construct *a posteriori*. However, the other models do not de-mean prior to inversion but do not agree with one another in the peak position of the distributions, thus it is not possible to explain this effect as a consequence of de-meaning the travel-time residuals alone. One might also expect the peak position, particularly when it is offset from zero in reality, to be affected by amplitude recovery issues inherent in every model (this is discussed further below) as well as differences in the kinds of damping used to condition the system of linear equations prior to inversion. To test whether amplitude recovery can explain differences in peak values we have attempted, without success, to find a correlation between total model amplitude variations and shifts in the peak positions of the distributions. Therefore we cannot offer any simple correction that brings model distributions into alignment, and in the following we consider the appropriate baseline value to be unconstrained. However, this issue by itself should not greatly affect the robustness of relative variations obtained in the inversions.

Table 4
Values of σ determined for different values of radial and lateral damping parameters, denoted λ_R and λ_L respectively

Depth λ_R, λ_L	3,4	4,3	4,4	4,5	5,4
1600 (km)	0.567	0.589	0.549	0.519	0.535
1800 (km)	0.588	0.597	0.569	0.547	0.551
2000 (km)	0.669	0.680	0.647	0.623	0.628
2200 (km)	0.661	0.673	0.629	0.600	0.614
2400 (km)	0.590	0.611	0.572	0.554	0.563
2600 (km)	0.671	0.697	0.647	0.617	0.641
2800 (km)	0.804	0.856	0.775	0.720	0.754

The modeled standard deviations of the Gaussian-like portions of the distributions σ also vary significantly in each model, as shown in Fig. 3. The standard deviation is clearly related to the ability of tomographic models to recover the amplitude of actual variations in seismic velocities in the dominant Gaussian portions of the models. We note that even in the absence of regularization (or "damping"), discretized tomographic models can only recover a lower bound on the total magnitude of actual velocity variations because it implicitly averages variations over a set of finite-sized volumes. The widths of the Gaussian distributions are related to the effective resolution of the inversions, with broader distributions mostly correlated with larger datasets. We attribute this to the fact that less well-resolved tomographic models require a greater degree of damping in order to avoid excessive stiffness and instability in the inversion process, and this has the effect of limiting the amplitude of model variations. We have explored this effect by varying both the lateral and radial damping parameters to obtain new distributions in the model HMSL, and the results of Gaussian fitting are shown in Table 4. While distributions obtained with different degrees of damping share the same features, the value of σ determined by the same Gaussian fitting procedure tends to decrease with increased damping, as expected. Clearly, this effect will also depend on the kind of conditioning employed in the model inversions, with the above example illustrating the effects of roughness damping.

The above-mentioned differences in peak amplitude and distribution widths between the models confounds a straightforward measure of Earth structure, however, information derived from the statistical distributions can be utilized in order to understand these differences and to

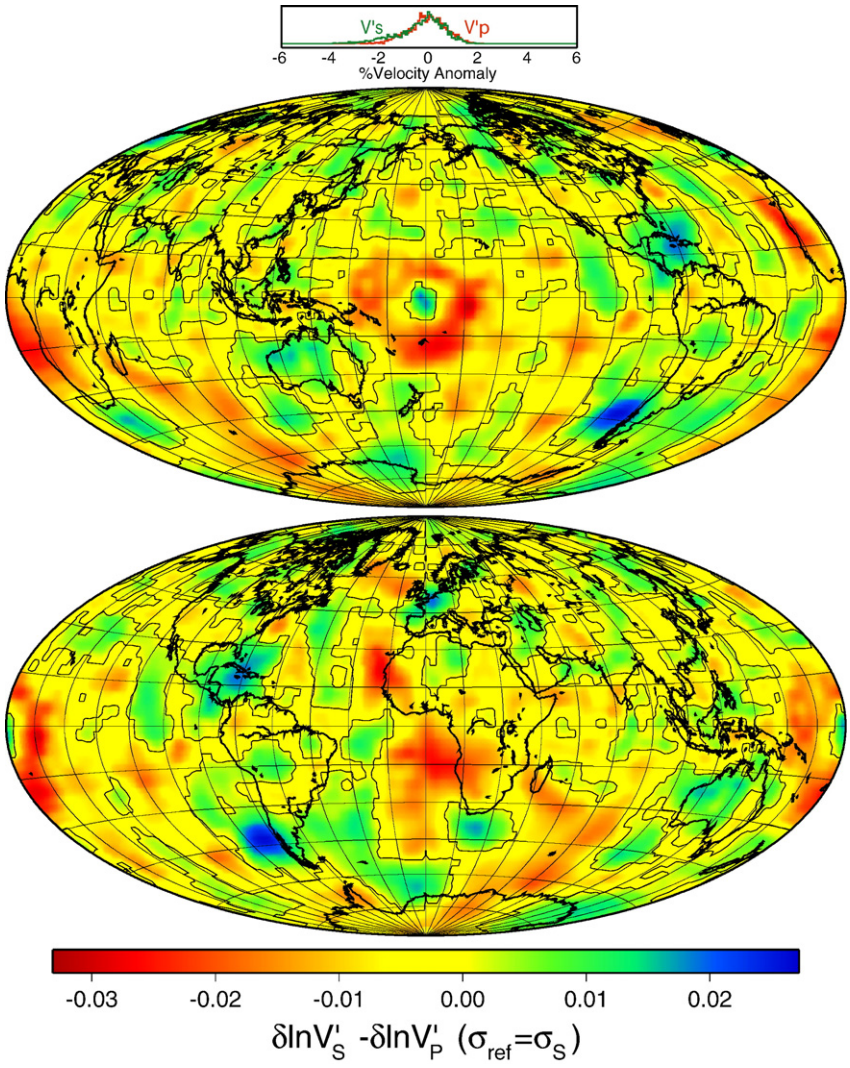

Fig. 4. Plot of $\delta \ln V_S' - \delta \ln V_P'$ in both hemispheres for model HMSL at 2600 km depth (see text for details), with the zero contour line drawn for reference. Positive values indicate where baseline shifted and scaled V_S exceeds the aligned and scaled V_P values, while negative values represent the converse. The distributions of $\delta \ln V_S'$ and $\delta \ln V_P'$ are also shown.

use these measures in model comparisons. For example, as a simple linear correction for amplitude and peak value differences one could apply a transformation of the form,

$$\delta \ln V_i' = \sigma_{\mathrm{ref}} \frac{\delta \ln V_i - \mu_i}{\sigma_i}, \quad (1)$$

where i denotes the ith model and $\delta \ln V_i'$ is a shifted and scaled version of each model with velocity amplitudes normalized to a reference standard deviation σ_{ref}. This brings the Gaussian-like portions of each distribution into both a similar alignment and scale, and takes advantage of the basic self-similarity in the form of the distributions. However, given the range of observed values of σ in the models, it is difficult to select an appropriate value of σ_{ref} with confidence that it corresponds to actual velocity variations in Earth's deep interior.

In order to recover relative S and P velocity amplitude variations with depth, one may compute $R_\sigma = \sigma_S/\sigma_P$ with σ_S and σ_P the standard deviations of the Gaussian portions of the S and P models respectively. Note that this definition for R_σ is similar to the ratio $R = \delta \ln V_S / \delta \ln V_P$, which has often been used to analyze relative variations in V_S and V_P in Earth's mantle. However, R_σ is more restricted because it only compares a portion of the distributions. Yet R_σ is also more robust than is R since it does not depend upon the baseline value and it is obtained by comparing dominant modal features in the global statistical distributions. For a given pair of V_P and V_S models, a nearly constant value of R_σ can be found

Table 5
Estimated volume of distinctly non-Gaussian anomalously low S velocity integrated from 2200–2891 km depth expressed as a fraction of total mantle volume

S model	Estimated volume
TX2006	2.4%
J362D28	1.9%
Houser	1.7%
S20RTS	2.1%
SAW24B16	1.9%
PRI-S05	1.5%
SMEAN	2.4%

throughout the lowermost mantle. On the other hand, this value is quite variable among the complete set of model pairs and a representative value cannot be singled out. Indeed, R_σ computed in this manner yields a range of about 1–4. We believe this result raises serious doubts regarding any notion that relative variations in V_S and V_P are well-constrained by tomographic model pairs alone.

Given the variations among models described above, it is even more difficult to compare V_S and V_P models in order to discern exactly how and where they differ in Earth's deep mantle. One potential method is to use the dominant Gaussian variations seen in each of the models, which would imply that the mechanism responsible for these variations is the same for both V_S and V_P models. For example, lacking any proper baseline reference for comparison, we could instead posit a correspondence between the most abundant velocities (i.e., peak positions) in P and S models. A particular comparison that would be expected to emphasize the low V_S tail between any two V_P and V_S maps would be to compute $\delta\ln V_S' - \delta\ln V_P'$ using $\sigma_{\mathrm{ref}} = \sigma_S$. This shifts the peak values of the S and P models to 0% and scales the P model so that the Gaussian-like portion is the same width as that of the S model. A plot of this kind is shown in Fig. 4 using HMSL-S06 and HMSL-P06. Regions where $\delta\ln V_S' - \delta\ln V_P' > 0$ indicate that V_S is increased relative to V_P, while $\delta\ln V_S' - \delta\ln V_P' < 0$ indicates regions where V_S slows relative to V_P, with the latter illustrating regions where the low V_S material manifests itself. Interestingly, there still exist regions where V_S is increased relative to V_P. As discussed in the next section, regions exhibiting low values of $\delta\ln V_S' - \delta\ln V_P'$ may be due to dense and chemically distinct material while regions exhibiting higher values may be indicative of post-perovskite-bearing rock.

3.2. Implications for Earth's deep mantle

The Gaussian fits allow us to estimate the areal coverage of the low V_S material at each depth, which can then be integrated over radius to yield the total volume of anomalously slow V_S material. Assuming the distribution to be the sum of two modes, we subtract the area of the dominant Gaussian feature and take the residual as our estimate of the areal coverage of low V_S material. The results of summing up to 2200 km depth from the CMB are summarized in Table 5 yielding anomalously slow V_S material occupying about $2.0 \pm 0.4\%$ of the total mantle volume. This value is comparable to the volume of continental lithosphere, and if these features are chemically anomalous this implies a similar capacity for storage of a geochemically distinct reservoir. These values are also comparable to estimates for the size and shape of low V_S material based on identifying ray paths for event-station pairs whose phase travel-time delays are significantly greater inside these features than outside (Wang and Wen, 2004).

Because temperature variations affect shear and compressional velocity in the same manner, a purely thermal origin for features in tomographic models

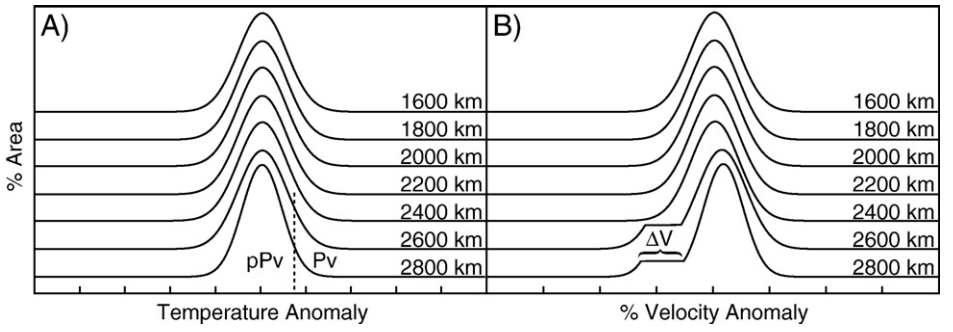

Fig. 5. Example of how Gaussian temperature anomalies at various depths (A) can lead to a low velocity tail in the distribution of V_S (B) if only the hottest material is in the Pv stability field while the remaining portions of the mantle are in the pPv stability field. The shift of ΔV between pPv and Pv only manifests at the greatest depths because this phase change is thought to be confined to the lowermost ≈300 km of the mantle. A baseline shift is applied schematically in B, such that the mean is zero.

would predict that V_S and V_P vary in a well-correlated manner that would also be present in the statistical distributions. The only similar feature in V_P and V_S models is the dominant Gaussian-like portions of the distributions, which are radially coherent throughout the lower mantle. As mentioned previously, if R_σ is estimated for most model pairs it is found that the width of the Gaussian feature in S models scales very similarly to the Gaussian variation in P models. On the other hand, one may also consider the change in the amplitude of individual seismic velocity variations with depth toward the CMB. Because the largest lateral temperature variations in Earth's outer core are estimated to be of order 10^{-4} K or less (Braginsky and Roberts, 1995), the CMB is an essentially isothermal surface. As a consequence, lateral temperature variations and their associated seismic signatures are expected to diminish with depth in the lower portion of the D'' layer as all regional geotherms converge to the same value at about 2891 km depth. If it is indeed possible to resolve this predicted feature, then the lack of a narrowing distribution of $\delta \ln V$ with depth (which would otherwise cause σ to decrease) suggests that chemical and/or phase heterogeneity at the very base of the mantle might be required to explain undiminished variations in the dominant Gaussian mode. Dynamic models of thermo-chemical convection (Tackley, 1998; Davaille et al., 2003; McNamara and Zhong, 2004) have all shown how a laterally discontinuous and compositionally dense layer can increase heterogeneity at the base of the mantle when the underlying CMB is isothermal. However, given that such a narrowing feature is likely difficult to resolve since the thermal boundary layer thickness is probably similar to or smaller than typical model discretizations, we suggest that this dominant mode of seismic velocity variations is most simply explained by the contribution of lateral temperature changes but cannot rule out some other contribution at the greatest depths.

Less straightforward is a simple explanation for the low V_S tail of the distributions, which is distinct from the behavior seen in all P models. There exists a large range of possible effects that might give rise to this feature, and it is therefore not uniquely determined by the form of the statistical distributions alone. Nevertheless, it is still possible to evaluate a number of options and see which are most compatible with independent constraints. We defer comparison to particular mantle convection models for later study since there exists a vast parameter space for such models within which a large number of factors could be found to reproduce the features noted in this study. However, some simple considerations may help to constrain the nature of this feature, which cannot be explained as thermal in origin.

It is worth considering whether a dimishinished V_S relative to V_P as revealed by the distributions could be explained by anharmonic and/or anelastic effects (Karato, 1993). It has been proposed that these effects may elevate the sensitivity of V_S to temperature variations in the lower mantle relative to V_P, thus explaining the apparent increase in the value of R (Karato and Karki, 2001). However, Karato and Karki (2001) find that below about 2000–2300 km depth another non-thermal contribution to lateral variations in V_S is likely necessary and cannot be explained by the combined anharmonic and anelastic effects, in good agreement with the depth of onset for the low V_S tail in the seismic velocity distributions. In any case, the steadiness of R_σ with depth implies that such effects might not be of great importance in Earth's mantle.

An intriguing possibility is that uncoupled lateral variations in V_S and V_P might be explained by lateral variations in the presence of post-perovskite (pPv) via a phase change from a perovskite (Pv) dominated phase assemblage at lower pressure and higher temperatures. Estimates of a velocity jump up to several percent in V_S and almost no change in V_P for the Pv–pPv transition appear to be compatible with the presence of seismically observed discontinuities near the top of the D'' layer (Iitaka et al., 2004; Tsuchiya et al., 2004; Wookey et al., 2005; Hirose, 2006). It could therefore be suggested that uncoupled changes in V_S and V_P can be explained by lateral variations in the occurrence of pPv-bearing rock. In other words, LLSVPs might simply be regions with little or no pPv, hence explaining their relatively small V_S relative to surrounding mantle with less dramatic variations in V_P. This effect could be amplified if pPv-bearing rock appears in extensive lens-like patches above the CMB which are bounded above, below, and along their edges by Pv-dominated rock with a correspondingly smaller V_S (Hernlund et al., 2005). Fig. 5 illustrates how this scenario might operate given Gaussian temperature anomalies, and with only the hottest material outside the pPv stability field. V_S would be increased by an amount ΔV in most of the material cool enough to be inside the pPv stability field provided the pressure is great enough, while the hottest material as well as mantle at shallower depths would be in the Pv stability field and hence intrinsically slower. An immediate problem with a pPv origin for the low shear velocity features seen in the statistical distributions is their depth extent. In particular, the upper discontinuity attributed to pPv is typically estimated to shallow to around 250–300 km (for a review, see

Wysession et al., 1998), and possibly as much 400 km above the CMB (e.g., Kendall and Shearer, 1994). This agrees with phase boundaries estimated from diamond anvil cell and ab initio models which predict a transformation from Pv to pPv at similar depths for temperatures around 3000 K (Hirose, 2006). While the shallowest reported values of observed discontinuities are uncorroborated by other seismic studies, even such extreme upward displacements are not as large as those required to explain the upward extension of the low V_S tail observed in the statistical distributions, which manifest themselves up to (and perhaps more than) 700 km above the CMB. This discrepancy of 400 km or more is large enough that it mediates any concern that the upward extension of the low V_S tail is an artifact of radial smearing. Thus while a pPv mechanism could potentially produce a low velocity hump like those seen in V_S distributions (Fig. 1) and a lack of such behavior in V_P distributions, it is only applicable between about 2600–2800 km depth because the pPv phase boundary is expected to be at much lower than attainable temperatures at depths shallower than about 2500 km (Hirose, 2006; Hernlund and Labrosse, 2007).

Forward models of mantle convection including a layer of chemically distinct and relatively dense material reveal striking similarities with the two LLSVP imaged in the deep mantle (e.g., Tackley, 1998, 2002; McNamara and Zhong, 2004; Tan and Gurnis, 2005). In these models, a modestly (1–3%) higher density layer is swept up into "chemical piles" away from downwelling slabs, in good agreement with the observed location and shape of the mid-Pacific and African LLSVP based on convection calculations with imposed plate motion history (McNamara and Zhong, 2005). Recently, high density reflectivity surveys detected pairs of discontinuities inside the Pacific LLSVP that are remarkably consistent with the presence of a post-perovskite (pPv) lens (Lay et al., 2006). The occurrence of pPv inside LLSVP is also supported by Sun et al. (2007) who observe an S triplication in the African structure. However, the existence of pPv in these generally slower regions at depths similar to the same kinds of structures detected in seismically faster regions (Thomas et al., 2004a,b; Hernlund et al., 2005; Sun et al., 2006; van der Hilst et al., 2007) also suggests that LLSVP may have a distinct chemistry that modulates the stability of pPv and allows it to be stabilized at slightly higher temperatures than conditions prevailing in the surrounding mantle. While it would be of interest to estimate the seismic velocity contributions required of variable chemistry to produce the low V_S tails, we note that such regions will have higher temperatures since they are likely stable and rest upon core while losing heat mostly via slow conduction into the surrounding mantle (e.g., McNamara and Zhong, 2005; Tan and Gurnis, 2005). Thus these regions require both a thermal and chemical contribution to seismic velocity variations, neither of which is well-constrained. Furthermore, the differences in the amplitudes of these features among the various models confound any attempt to identify a single value representative of actual variations in the mantle.

Our favored interpretation of the relative V_S and V_P differences revealed in Fig. 4 using $\delta\ln V_S' - \delta\ln V_P'$ is that regions of higher V_S values may contain pPv-bearing rock, while the slower V_S regions are consistent with chemically distinct dense material. We note that the occurrence of high $\delta\ln V_S' - \delta\ln V_P'$ in the interiors of the African and Pacific LLSVP (showing bulls-eye like patterns) is not well-resolved by P models, although these are intriguing features that might be compatible with the occurrence of pPv lenses inside chemically distinct LLSVP, as discussed previously. It is clear that better coverage in all types of seismic tomography models, further improvements in inversion techniques, and careful examination of the resulting models using simple techniques like those described here will increase the quality of interpretations for mantle structure and its implications for mantle dynamics and evolution.

We finally note that other explanations for LLSVPs persist and give reason to question the uniqueness of any interpretation involving differences in chemistry and/or phase. For example, LLSVPs have been proposed to be large thermal "super-plumes" whose broad structure is a consequence of a smaller effective convective vigor due to enhanced thermal conductivity, higher viscosity, or smaller thermal expansivity in the deep mantle (e.g., Matyska et al., 1994). Likewise, the opposite scenario has been proposed where an enhanced convective instability in D'' leads to concentrated clusters of small thermal plumes that are swept together by the plate-scale circulation to regions away from subduction zones (Schubert et al., 2004). Neither of these scenarios can explain the pronounced decrease in V_S relative to V_P as evidenced in the statistical distributions, nor do they explain the localization of ultralow-velocity zones at the edges of the LLSVPs (Thorne et al., 2004), or the appearance of discontinuities compatible with the occurrence of pPv-bearing rock (Lay et al., 2006; Sun et al., 2007).

4. Conclusion

We have established that the observations of a nearly bimodal distribution in shear velocities and the lack thereof in compressional velocities are robust features of the deep

mantle, extend radially to 700 km or more above the core–mantle boundary, and occupy a volume that is $\approx 2 \pm 0.4\%$ of Earth's mantle. The signature can only partly be explained by lateral variations in pPv-bearing rock because the pPv stability is thought to be confined to within about 300 km of the CMB for reasonable temperatures in Earth's deep interior (Hernlund and Labrosse, 2007). Model comparisons guided by the statistical distributions of seismic velocity offers useful insights into differences in V_S and V_P in Earth's deep interior that may be diagnostic of chemically distinct material as well as occurrences of pPv-bearing rock. Further improvements in the resolution of P tomography models, soon to be realized by the incorporation of the P_{diff} and other phases, will offer ever more powerful constraints on the structure of Earth's deep mantle and on the planform and nature of mantle convection.

Acknowledgments

We thank Lapo Boschi, Saskia Goes, Claude Jaupart, Mark Jellinek, Stéphane Labrosse, Jeroen Ritsema, Frederick Simons, and Paul Tackley for their valuable discussions, and Thorsten W. Becker, Nathan Simmons, and an anonymous reviewer for their thorough and enlightening reviews. JWH was supported by the French Ministry of Research and a CIAR post-doctoral fellowship. CH was supported by the UC President's Postdoctoral Fellowship Program.

References

Antolik, M., Gu, Y., Ekstrom, G., Dziewonski, A., 2003. J362d28: a new joint model of compressional and shear velocity in the Earth's mantle. Geophys. J. Int. 153, 443–466.

Becker, T.W., Boschi, L., 2002. A comparison of tomographic and geodynamic mantle models. Geochem. Geophys. Geosyst. 3 2001GC000168.

Beghein, C., Resovsky, J., Trampert, J., 2002. P and S tomography using normal-mode and surface wave data with a neighbourhood algorithm. Geophys. J. Int. 149, 646–658.

Birch, F., 1952. Elasticity and constitution of the earth's interior. J. Geophys. Res. 57, 227–286.

Bolton, H., Masters, G., 2001. Travel times of P and S from the global digital seismic networks: implications for the relative variation of P and S velocity in the mantle. J. Geophys. Res. 106, 13527–13540.

Braginsky, S.I., Roberts, P.H., 1995. Equations governing convection in Earths core and the geodynamo. Geophys. Astrophys. Fluid Dyn. 79, 1–97.

Bullen, K.E., 1949. Compressibility-pressure hypothesis and the Earth's interior. Mon. Not. R. Astron. Soc. Geophys. Suppl. 5, 355–368.

Davaille, A., Le Bars, M., Carbonne, C., 2003. Thermal convection in a heterogeneous mantle. C. R. Geosci. 335, 141–156.

Davies, J.H., Bunge, H.-P., 2001. Seismically "fast" geodynamic models. Geophys. Res. Lett. 28, 73–76.

Dziewonski, A.M., Anderson, D.L., 1981. Preliminary reference earth model. Phys. Earth Planet. Inter. 25, 297–356.

Ekstrom, G., Tromp, J., Larson, E.W.F., 1997. Measurements and global models of surface wave propagation. J. Geophys. Res. 102, 8137–8157.

Forte, A.M., Mitrovica, J.X., 2001. Deep-mantle high-viscosity flow and thermochemical structure inferred from seismic and geodynamic data. Nature 410, 1049–1056.

Gu, Y., Dziewonski, A.M., Su, W., Ekstrom, G., 2001. Models of mantle shear velocity and discontinuities in the pattern of lateral heterogeneities. J. Geophys. Res. 106, 11,169–11,199.

Hager, B.H., Clayton, R.W., 1989. Constraints on the structure of mantle convection using seismic observations, flow models, and the geoid. In: Peltier, W.R. (Ed.), Mantle Convection; Plate Tectonics and Global Dynamics. Gordon and Breach Science Publishers, pp. 657–763.

Hernlund, J.W., Labrosse, S., 2007. Geophysically consistent values of the perovskite to post-perovskite transition Clapeyron slope. Geophys. Res. Lett. 34, L05309. doi:10.1029/2006GL028961.

Hernlund, J.W., Thomas, C., Tackley, P.J., 2005. A doubling of the post-perovskite phase boundary and structure of the Earth's lowermost mantle. Nature 434, 882–886. doi:10.1038/nature03472.

Hirose, K., 2006. Postperovskite phase transition and its geophysical implications. Rev. Geophys. 44, RG3001. doi:10.1029/2005RG000186.

Hofmann, A.W., 1997. Mantle geochemistry: the message from oceanic volcanism. Nature 385, 219–229.

Houser, C., Masters, G., Shearer, P., Laske, G., submitted for publication. Shear and compressional velocity model of the mantle from cluster analysis of long-period waveforms. Geophys. J. Int.

Iitaka, T., Hirose, K., Kawamura, K., Murakami, M., 2004. The elasticity of the MgSiO3 post-perovskite phase in the Earth's lowermost mantle. Nature 430, 442–445.

Ishii, M., Tromp, J., 2004. Constraining large-scale mantle heterogeneity using mantle and inner-core sensitive modes. Phys. Earth Planet. Inter. 146, 113–124.

Karato, S., 1993. Importance of anelasticity in the interpretation of seismic tomography. Geophys. Res. Lett. 20, 1623–1626.

Karato, S., Karki, B.B., 2001. Origin of lateral heterogeneity in seismic wave velocities and density in Earths deep mantle. J. Geophys. Res. 106, 21771–21783.

Kendall, J.-M., Shearer, P.M., 1994. Lateral variations in D'' thickness from long-period shear wave data. J. Geophys. Res. 99, 11575–11590.

Kennett, B.L.N., Engdahl, E.R., 1991. Traveltimes for global earthquake location and phase identification. Geophys. J. Int. 105, 429–465.

Kennett, B.L.N., Engdahl, E.R., Buland, R., 1995. Constraints on seismic velocities in the Earth from travel times. Geophys. J. Int. 122, 108–124.

Kennett, B.L.N., Widiyantoro, S., van der Hilst, R.D., 1998. Joint seismic tomography for bulk sound and shear wave speed in the Earth's mantle. J. Geophys. Res. 103, 12469–12493.

Lay, T., Hernlund, J., Garnero, E.J., Thorne, M.S., 2006. A post-perovskite lens and D'' heat flux beneath the central Pacific. Science 314, 1272–1276. doi:10.1126/science. 1133280.

Li, C., van der Hilst, R., in press. Geochem. Geophys. Geosyst.

Liu, X., Dziewonski, A.M., 1998. Global analysis of shear wave velocity anomalies in the lowermost mantle. In: Gurnis, M., Wysession, M.E., Knittle, E., Buffett, B.A. (Eds.), The Core–Mantle Boundary Region. American Geophysical Union Monograph, pp. 23–36.

Masters, G., Laske, G., Bolton, H., Dziewonski, A., 2000. The relative behavior of shear velocity, bulk sound speed, and compressional

velocity in the mantle: Implications for chemical and thermal structure, in Earth's Deep Interior. In: Karato, S.-I., Forte, A., Liebermann, R., Masters, G., Stixrude, L. (Eds.), Mineral Physics and Tomography from the Atomic to Global Scale. American Geophysical Union Monograph, pp. 63–87.

Matyska, C., Moser, J., Yuen, D.A., 1994. The potential influence of radiative heat transfer on the formation of megaplumes in the lower mantle. Earth Planet. Sci. Lett. 125, 255–266.

McNamara, A.K., Zhong, S., 2004. Thermochemical structures within a spherical mantle: Superplumes or piles? J. Geophys. Res., B 109, B07402.

McNamara, A.K., Zhong, S., 2005. Thermochemical piles under Africa and the Pacific. Nature 437, 1136–1139.

Megnin, C., Romanowicz, B., 2000. The three-dimensional shear velocity structure of the mantle from the inversion of body, surface, and higher-mode waveforms. Geophys. J. Int. 143, 709–728.

Montelli, R., Nolet, G., Dahlen, F.A., Masters, G., Engdahl, R., Hung, S.-H., 2004. Finitefrequency tomography reveals a variety of plumes in the mantle. Science 303, 338–343. doi:10.1126/science.1092485.

Montelli, R., Nolet, G., Dahlen, F.A., Masters, G., 2006. A catalogue of deep mantle plumes: new results from finite frequency tomography. Geochem. Geophys. Geosyst. 7. doi:10.1029/2006GC001248.

Ni, S., Tan, E., Gurnis, M., Helmberger, D., 2002. Sharp sides to the African superplume. Science 296, 1850–1852.

Ritsema, J., van Heijst, H.J., 2000. Seismic imaging of structural heterogeneity in Earth's mantle: evidence for large-scale mantle flow. Sci. Prog. 83, 243–259.

Ritsema, J., van Heijst, H.J., 2002. New constraints on the *P* velocity structure of the mantle from *P*, *PP*, *PPP*, and PKPab travel-times. Geophys. J. Int. 149, 482–489.

Robertson, G.S., Woodhouse, J.H., 1995. Evidence for proportionality of *P* and *S* heterogeneity in the lower mantle. Geophys. J. Int. 123, 85–116.

Robertson, G.S., Woodhouse, J.H., 1996. Ratio of relative *S*-to-*P*-velocity heterogeneity in the lower mantle. J. Geophys. Res. 11, 20041–20052.

Saltzer, R., van der Hilst, R.D., Karason, H., 2001. Comparing *P* and *S* wave heterogeneity in the mantle. Geophys. Res. Lett. 28, 1335–1338.

Schubert, G., Masters, G., Tackley, P.J., Olson, P., 2004. Superplumes or plume clusters? Phys. Earth Planet Inter. 146, 147–162.

Simmons, N.A., Forte, A.M., Grand, S.P., 2006. Constraining mantle flow with seismic and geodynamic data: a joint approach. Earth Planet. Sci. Lett. 246, 109–124. doi:10.1029/2006GL028009.

Simmons, N.A., Forte, A.M., Grand, S.P., 2007. Thermochemical structure and dynamics of the African superplume. Geophys. Res. Lett. 34, L02301. doi:10.1029/2006GL028009.

Su, W.J., Dziewonski, A.M., 1997. Simultaneous inversion for 3-D variations in shear and bulk velocity in the mantle. Phys. Earth Planet. Inter. 100, 135–156.

Sun, D., Song, T.-R.A., Helmberger, D., 2006. Complexity of *D″* in the presence of slab-debris and phase change. Geophys. Res. Lett. 33, L12S07. doi:10.1029/2005GL025384.

Sun, D., Tan, E., Helmberger, D., Gurnis, M., 2007. Seismological support for the metastable superplume model, sharp features, and phase changes within the lower mantle. Proc. Natl. Acad. Sci. 104, 9151–9155.

Tackley, P.J., 1998. Three-dimensional simulations of mantle convection with a thermo-chemical basal boundary layer: D″? In: Gurnis, M., Wysession, M.E., Knittle, E., Buffett, B.A. (Eds.), The Core–Mantle Boundary Region. American Geophysical Union Monograph, pp. 231–253.

Tackley, P.J., 2002. Strong heterogeneity caused by deep mantle layering. Geochem. Geophys. Geosyst. 3. doi:10.1029/2001GC000167.

Tan, E., Gurnis, M., 2005. Metastable superplumes and mantle compressibility. Geophys. Res. Lett. 32, L20307. doi:10.1029/2005GL024190.

Thomas, C., Garnero, E.J., Lay, T., 2004a. High-resolution imaging of lowermost mantle structure under the Cocos plate. J. Geophys. Res., B 109, B08307.

Thomas, C., Kendall, J., Lowman, J., 2004b. Lower-mantle seismic discontinuities and the thermal morphology of subducted slabs. Earth Planet. Sci. Lett. 225, 105–113.

Thorne, M., Garnero, E.J., Grand, S., 2004. Geographic correlation between hot spots and deep mantle lateral shear-wave velocity gradients. Phys. Earth Planet. Inter. 146, 47–63.

Trampert, J., Deschamps, F., Resovsky, J., Yuen, D.A., 2004. Probabilistic tomography maps chemical heterogenities throughout the mantle. Science 306, 853–856.

Tsuchiya, T., Tsuchiya, J., Umemoto, K., Wetzcovitch, R.M., 2004. Elasticity of post-perovskite MgSiO3. Geophys. Res. Lett. 31, L14603.

van der Hilst, R.D., de Hoop, M.V., Wang, P., Shim, S.-H., Ma, P., Tenorio, L., 2007. Seismostratigraphy and thermal structure of Earth's core-mantle boundary region. Science 30, 1813–1817. doi:10.1126/science.1137867.

Vasco, D.W., Johnson, L.R., Pulliam, R.J., Earle, P.S., 1994. Robust inversion of IASP91 travel time residuals for mantle *P* and *S* velocity structure, earthquake mislocations, and station corrections. J. Geophys. Res. 99, 13727–13755.

Wang, Y., Wen, L., 2004. Mapping the geometry and geographic distribution of a very low velocity province at the base of the Earth's mantle. J. Geophys. Res. 109, B10305.

Wen, L., 2001. Seismic evidence for a rapidly-varying compositional anomaly at the base of the Earth's mantle beneath the Indian ocean. Earth Planet. Sci. Lett. 194, 83–95.

Woodhouse, J.H., Dziewonski, A.M., 1984. Mapping the upper mantle: three-dimensional modeling of earth structure by inversion of seismic waveforms. J. Geophys. Res. 89, 5953–5986.

Wookey, J., Stackhouse, S., Kendall, J.-M., Brodholt, J., Price, G.D., 2005. Efficacy of the post-perovskite phase as an explanation of lowermost mantle seismic properties. Nature 438, 1004–1008.

Wysession, M.E., Lay, T., Revenaugh, J., Williams, Q., Garnero, E.J., Jeanloz, R., Kellogg, L.H., 1998. The *D″* discontinuity and its implications. In: Gurnis, M., Wysession, M.E., Knittle, E., Buffett, B.A. (Eds.), The Core–Mantle Boundary Region. American Geophysical Union Monograph, pp. 273–297.

Yanagisawa, T., Hamano, Y., 1999. "Skewness" of *S*-wave velocity in the mantle. Geophys. Res. Lett. 26, 791–794.